

## Admittance spectroscopy of 2–5 nm detonation diamonds in NaCl-nanodiamond mixture. Electronic properties of small nanodiamonds

S.G. Buga<sup>a,b,\*</sup>, M.Yu. Popov<sup>c</sup>, D.A. Ovsyannikov<sup>a</sup>, V.S. Baidyshev<sup>d</sup>, A.G. Kvashnin<sup>d</sup>

<sup>a</sup> Research Center "Kurchatov Institute"-TISNUM, Moscow, Russia

<sup>b</sup> Moscow Center for Advanced Studies, 107031, Moscow, Russia

<sup>c</sup> Prokhorov General Physics Institute of the Russian Academy of Sciences, Moscow, Russia

<sup>d</sup> Skolkovo Institute of Science and Technology, Moscow, Russia

### ARTICLE INFO

#### Keywords:

Nanodiamond  
Admittance spectroscopy  
Activation energy of charge carriers  
Band structure  
DFT simulations

### ABSTRACT

The complex electrical conductivity of detonation diamonds with a size of 2–5 nm in a NaCl dielectric matrix was studied in the temperature range  $T = 300\text{--}400$  K and in the frequency range of  $10^3\text{--}10^7$  Hz with an amplitude of the alternating current of 30 mV. The concentration range of nanodiamonds in the studied samples was from 0.16 to 59 vol%. The steps in the frequency dependence of the electrical capacitance  $C(f)$ , and the maxima in the reduced conductivity  $G_{\omega}(f)$  at fixed values of  $T$  were revealed, making it possible to use admittance spectroscopy method to determine the emission rate, activation energy, and capture cross-section of charge carriers in nanodiamonds. For the three concentrations of ND: 17, 48, and 59 vol% the value of  $E_a = 0.19 \pm 0.02$  eV is obtained. The emission rate at 300 K was  $10^4 \text{ s}^{-1}$  while the capture cross-section was  $(2.5 \pm 0.5) \times 10^{-20} \text{ cm}^2$ . This indicates the hopping conduction mechanism with the conductivity of  $\sim 10^{-6} \Omega^{-1} \text{ cm}^{-1}$ . The concentration of charge carriers at 300 K is estimated to be in the range of  $10^{12}\text{--}10^{13} \text{ cm}^{-3}$ . A density functional study of the electronic properties of diamond nanoclusters of different sizes is performed. The calculated electronic densities of states for clusters with diameters ranging from 0.8 to 1.7 nm show a strong dependence on the size and surface reconstruction.

### 1. Introduction

Physical properties of nanodiamonds (ND) differ greatly from those of macroscopic and micron-sized diamonds due to the large fraction of surface atoms and the possibility of adsorption of other atoms and radicals on them [1–8]. This has opened up a wide range of their applications in various fields of modern technology, for example, as useful additives and modifiers for many industrial liquid and solid chemical compounds, components of optoelectronic and quantum electronic systems, as well as means of biomedical imaging and drug delivery sensing.

The smallest 2–5 nm nanodiamonds are produced on industrial scales using the detonation technology of oxygen-deficient explosives in an inert atmosphere inside specially constructed steel detonation chambers [8,9]. As a result of detonation, a shock wave propagates through the reaction mixture at supersonic speed, creating a pressure of up to 10–20 GPa and a temperature of up to 2000–4000 K, which favors the synthesis of detonation nanodiamonds (DND).

The powdery mixture of products from the detonation is cleaned with acids and reagents to remove metallic impurities and soot. The resulting DNDs are commercially available as a powder or as a suspension in water. However, rough DND particles usually are aggregated in large blocks  $\sim 100$  nm in size [10]. The as-supplied material thus requires deaggregation into its constituent particles before subsequent processing. Deaggregation is usually achieved by ball milling, pulverization, high-power sonication, acid treatments, controlled heating in  $O_2$  or  $H_2$ , or combinations of these methods. Nevertheless, the target material – purified and deaggregated DND never look like totally  $sp^3$  bonded nanoclusters, there are fractions of  $sp^2$  and hybrid  $sp^2/sp^3$  bonded atoms on DND surface [3,4]. Nuclear magnetic resonance (NMR) of DND of sizes 5.2, 6.2, 7.6 nm [3] and parallel electron energy loss spectroscopy (PEELS) of a 4.8 nm DND [4] showed that less than 50 % of carbon atoms form the core of ND, as in the bulk of a crystalline diamond, while more than 50 % of atoms locate in their outer layers with distorted  $sp^3$  bonds. And about 1 % of atoms on the surface of such DND have combined  $sp^2/sp^3$  bonds and  $\pi$  electrons. It is important to

\* Corresponding author at: Research Center "Kurchatov Institute"-TISNUM, Moscow, Russia.

E-mail address: [buga@tisnum.ru](mailto:buga@tisnum.ru) (S.G. Buga).

note, that Raman spectra of purified DND [11,7] confirmed an absence of graphite shell covering nanodiamond grain. Thus, it is expected that electrical properties of purified DND must be semiconductor, not semimetal.

Density functional theory (DFT) and Molecular Mechanics (MM) computational models of DND [12–14] complemented the experimental data [3,4,13] related to their structure, however, there is still a lack of the data regarding electrical charge transport in DND, in particular, the electrical conductivity, activation energy of charge carriers, band structure and the density of electronic states (DOS).

A well-known method for studying the electrical properties of various nanopowders is the method of measuring electrical impedance or admittance at low amplitude alternating current (AC) using mixtures of nanopowders with a dielectric binder [15]. In this case, it is possible to measure the electrical properties of nanopowders despite the presence of an energy barrier caused by a dielectric binder, like NaCl, for example. The admittance spectroscopy method [16] is also widely used to study impurity states in wide-bandgap semiconductors, such as phosphorus-doped diamonds [17], boron-containing natural and synthetic diamonds [18,19], and GaP [20].

In this work we studied the electrical admittance of purified ball-milled DND with an average size of 2–5 nm in a composition with NaCl as a dielectric binder. Using the admittance spectroscopy method with heating of samples in the range of 300–400 K, we determined the value of the thermal ionization energy of the charge carriers  $E_a$ , their emission rate  $e_n$ , and capture cross-section  $\delta_n$ . DFT calculations were used to obtain the dependence of the density of electronic states for diamond nanoclusters with the size from 96 to 465 atoms, which corresponds to a radius of up to 1.7 nm.

## 2. Experimental samples and methods

For the research, ND + NaCl mixtures in the concentration range of 0.16–59 vol% ND were prepared, obtained by processing in a ball mill, similar to Refs. [5–7]. We used purified 2–5 nm DND produced by the SANTA company (Brest, Republic of Belarus) for the study. To prevent contamination and adsorption of water on the surface, nanodiamonds were annealed in vacuum at a temperature of 600 °C, and then, together with pure NaCl in various concentrations, they were processed in a planetary ball mill in a nitrogen atmosphere. Containers and beads of the mill were made of silicon nitride. The treatment mode was chosen in such a way that non-carbon atoms from the surface of nanodiamonds diffused into NaCl. As noted in [5], after such treatment, neither C—O bonds nor adsorbed oxygen were observed in the XPS spectra of nanodiamonds. A 20-min treatment in a ball mill made it possible to obtain homogeneous mixtures without contamination with SiN balls material. After the processing, the ND + NaCl powders were compacted into tablets with a diameter of 12 mm and a thickness ranging from 1.6 to 2.2 mm in an inert atmosphere. In addition, similar test samples were prepared from the original pure NaCl, from NaCl processed in the same mill, as well as from a conventional mechanical mixture (without using a ball mill) ND + NaCl in a ratio of 50/50 wt%. Electrical contacts Ø 10 mm to the samples were made with a silver conductive paste cured at  $T = 50$  °C. Electrical measurements were performed using a Kethley-4200-SCS meter of electrical properties of semiconductor materials in the frequency range  $f = 10$  kHz–10 MHz with an AC voltage amplitude of 30 mV in the mode of an equivalent circuit for parallel connection of the intrinsic capacitance of nanodiamonds  $C_1$  and their resistance in the form of a resistor  $R$  with a series-connected large capacitance  $C_2 \gg C_1$  in the form of a NaCl layer between metal contacts and nanodiamonds. Such an equivalent electrical circuit of the samples was selected based on the analysis of Cole-Cole diagrams, examples of which are given in Appendix.

To determine the activation energy of charge carriers, their emission rate, and capture cross-section, the effect of heating to  $T = 400$  K on the frequency dependences of conductance  $G(f)$  and capacitance  $C(f)$  of

samples with a volume fraction of 17, 48, and 59 vol% ND was investigated in a Linkam-1000TS heating stage filled with pure dry argon.

## 3. Computational details

Geometry optimization of diamond nanoclusters are performed in the framework of density functional theory [21,22] by using VASP package [23–25] within the generalized gradient approximation (the Perdew–Burke–Ernzerhof functional) [26] and the projector augmented wave method [27,28]. The plane-wave energy cutoff was set to 400 eV. Atomic structure minimization is carried out until the change in total energy is less than  $10^{-4}$  eV. The vacuum distance between the periodic images of the clusters was set to 20 Å in each direction to avoid the artificial interaction between periodic images of the clusters.

## 4. Experimental results

Fig. 1(a) and (b) show the frequency dependences of the conductance  $G$  and the capacity of samples  $C$  of compacts with different ND contents, multiplied on the thickness  $t$  of samples for the correct comparison of the data obtained, and the real part of the dielectric constant  $\epsilon'$  (Fig. 1(a), right axes) at  $T = 298$  K. Fig. 1(c) demonstrates the frequency dependences of the reduced conductance  $G_\omega = G/\omega$  also at  $T = 298$  K, taking into account thicknesses of samples  $t$  as well. The dependences of  $C(f)$  and  $G_\omega(f)$  for a sample with 59 vol% ND at three temperature values:  $T = 25, 50$ , and  $90$  °C (as examples) are presented in Fig. 1(d). The same dependences were investigated for samples with 17 and 48 vol % ND. It is worth noting, that y-axes in Fig. 1(a–c) are logarithmic for better comparison of different samples, while in Fig. 1(d) – linear, according to the admittance spectroscopy method.

According to the theory of admittance spectroscopy of semiconductors [15,16], the frequency  $f_{\max}$  of the maximum of reduced conductivity  $G_\omega(f)$  depends on temperature, and the maximum occurs when the characteristic rates  $e_n$  of excitation and capture of charge carriers are equal. In this case  $f_{\max}$  is twice as high as  $e_n$ :

$$f_{\max} = 2e_n \quad (1)$$

$$e_n = \Gamma \delta_n T^2 \exp(-E_a/k_B T); \quad (2)$$

where  $\Gamma = (2\pi)^3/3^{1/2}m_e^*h^{-3}k_B^2$ ;

$m_e^*$  - effective mass of charge carriers;  $E_a$  – activation energy;  $\delta_n$  – their capture cross-section;  $h$  – Plank constant;  $k_B$  – Boltzmann constant.

The frequency of the maximum of the reduced conductivity corresponds to the middle of the “step” of the capacitance  $C(f)$  at the same temperature [15,16], and the ratio of the amplitude of the maximum  $G_\omega(f)$  and the value of  $C(f)$  in the low frequency range should be 1:2. In our case, this ratio is about 1:3, which can be explained by the influence of NaCl compound on the measurement results. Based on the dependences obtained, the values of  $f_{\max}$  at fixed temperature values were determined, and graphs of the dependences of  $f_{\max}/T^2$  on the inverse temperature  $1/T$  in Arrhenius coordinates were plotted for 3 samples with different content of ND (Fig. 2) to determine the activation energy of charge carriers in accordance with the admittance spectroscopy method.

The average value of  $E_a = 0.19 \pm 0.02$  eV is found from the data for samples with 17, 48, and 59 vol% of ND in mixture with NaCl (Fig. 2). Knowing  $E_a$  and  $f_{\max}$  we calculated  $\delta_n = (2.5 \pm 0.5) \times 10^{-20}$  cm<sup>2</sup> at  $T = 300$  K in accordance with relation (2). The small value indicates high degree of localization of charge carriers, as happens in highly B-doped diamonds at temperatures below ~150 K [18], where the values down to  $4 \times 10^{-22}$  cm<sup>2</sup> were found. In such a case hole transport occurs within the acceptor impurity band via the hopping mechanism. Accordingly, the low emission rates  $e_n$  of the order of  $(10^3\text{--}10^5)$  s<sup>-1</sup> were reported. In our case this parameter is of the order of  $(10^3\text{--}10^4)$  s<sup>-1</sup>, as follows from Fig. 1(d) and relation (1).

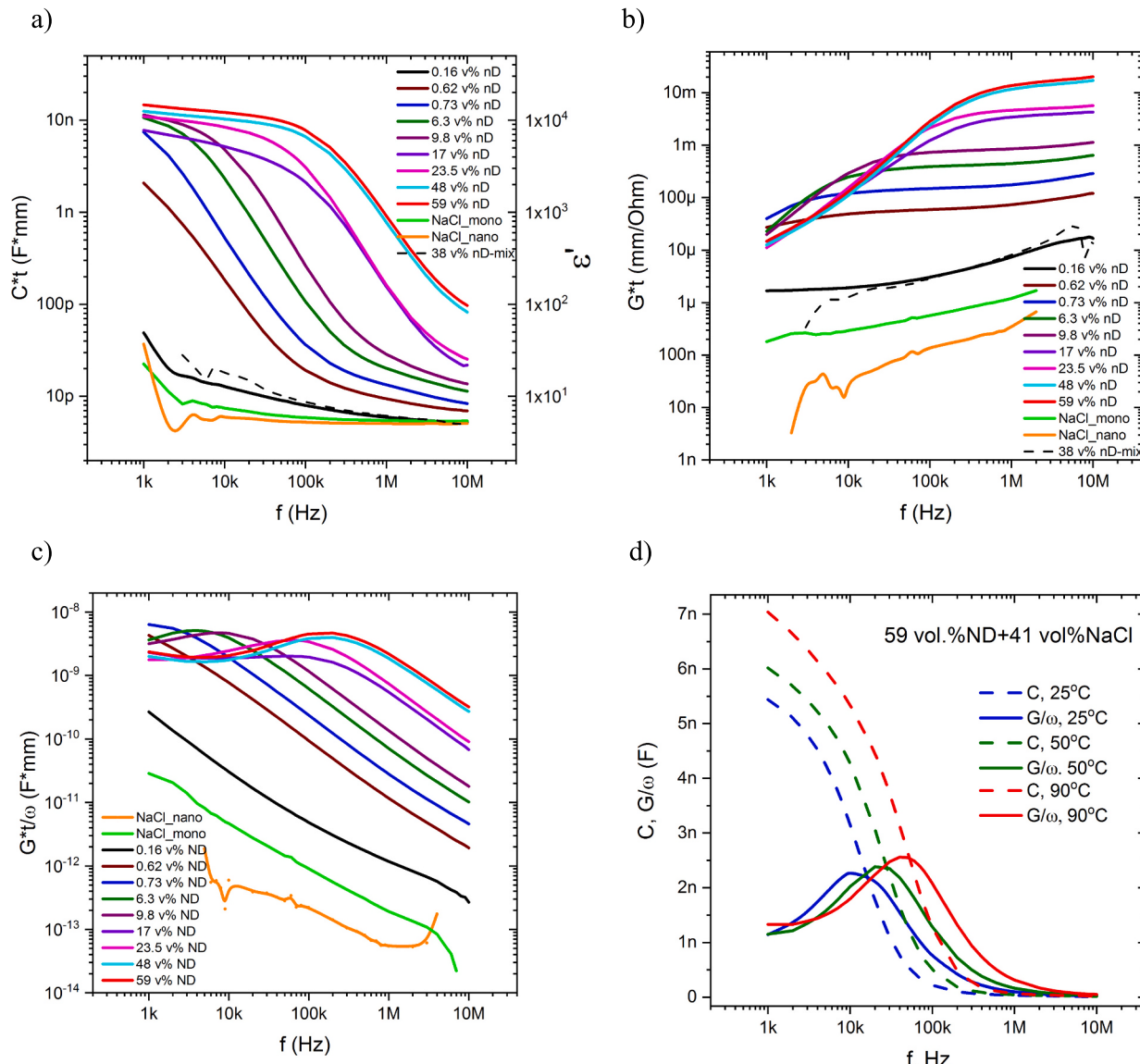


**Fig. 1.** Frequency dependences of capacity of the samples multiplied on their thickness (a), conductance (b), conductance reduced to the angular frequency (c), all data collected at  $T = 297$  K, volume concentrations of ND are indicated in the plots; capacity and reduced conductance of the sample with 59 vol% DND at  $T = 25$ ; 50; 90 °C (d).

As can be seen from Fig. 1(a), the measured dielectric constant of a sample from the initial monocrystalline NaCl at  $f > 100$  kHz approaches the known value  $\epsilon = 6.3$ . For a sample made from pure NaCl after processing in a ball mill, this value is slightly lower over the entire frequency range and approaches the tabular value in the frequency range 2 kHz - 10 MHz. The addition of 0.16 vol% ND leads to a noticeable increase in  $\epsilon$ . The conductance of a sample made of pure NaCl after processing in a ball mill is several times lower than that of a sample made of monocrystalline NaCl, however, the addition of 0.16 vol% ND dramatically increases the value of  $G$  by almost 2 orders of magnitude. It is important to note that the addition of 38 vol% (that is 50 wt%) ND by simple mechanical mixing without grinding in a ball mill has several orders of magnitude less effect on the values of capacitance and conductance over the entire frequency range studied, than, for example, addition of 23–48 vol% ND and processing in the mill. In fact, the  $C(f)$  and  $G(f)$  dependences for a sample with 38 vol% ND obtained by simple mechanical mixing without grinding in a ball mill coincide with such dependences for a sample containing 0.16 vol% ND but compacted from a mixture processed in the mill.

As shown in Figs. 1(a,b), the main trend with an increase in the

concentration of ND in the samples is an increase in the values of  $C$ ,  $G$  and  $\epsilon$ . At the same time, the opposite trend is observed in the frequency range below 30 kHz: the conductivity of samples at fixed frequency values decreases with increasing ND concentration (with the exception of 0.16 vol% ND). However, the dependences for the reduced conductivity in Fig. 1(c) shows that this “effect” is caused by a shift of the resonant peak towards higher frequencies with an increase in ND concentration, and at ND concentrations of less than 6 vol%, this maximum is located in the frequency range  $f < 1$  kHz. Consequently, the low-frequency value  $G/\omega$  for such samples should also be lower than in samples with a high concentration of ND. For concentrations of ND 48–59 vol%, approximately the same value of conductance is observed at a frequency of 500 Hz, that can be approximated as DC conductance:  $G \approx 3 \times 10^{-6} \Omega^{-1}$ , corresponding to a conductivity of  $\sigma \approx 10^{-6} (\Omega \text{ cm})^{-1}$ . If we assume that the mobility of charge carriers due to the conduction over localized states at  $T = 300$ – $400$  K is of the order of  $\mu \sim (1 \div 10) \text{ cm}^2/\text{Vs}$ , then from the known ratio for DC conductivity  $\sigma = e\mu n$ , where  $e$  is the electron charge and  $n$  is the concentration of charge carriers, the value of  $n \approx (10^{12} \div 10^{13}) \text{ cm}^{-3}$  can be obtained.

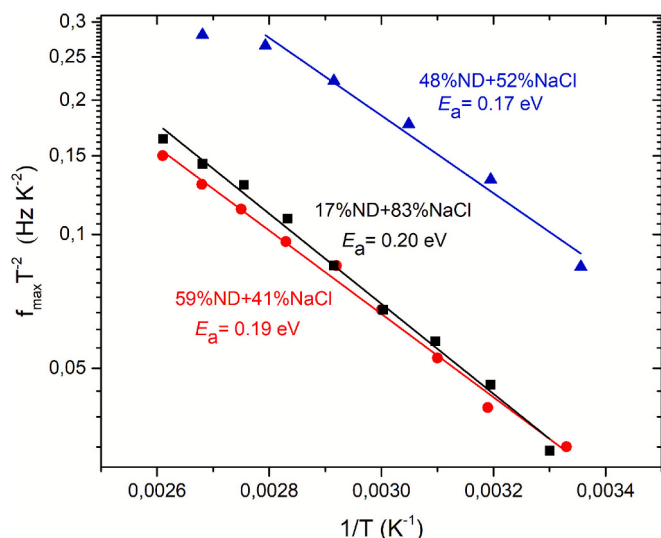


Fig. 2. Dependences of  $f_{\max}/T^2$  on  $1/T$  in Arrhenius coordinates for samples with 17, 48, and 59 vol% ND.

## 5. Results of simulations

To study how significantly the electronic properties of nanodiamonds can vary depending on the size, simulations based on the density functional theory are performed. Six types of diamond nanoclusters are considered having the average diameters (size) of 0.8, 1, 1.2, 1.5, 1.6, and 1.7 nm (96, 159, 250, 342, 378, and 465 carbon atoms). Each cluster is cut out of the single crystal bulk diamond structure and then relaxed by using DFT. The surface of each cluster is partially distorted during relaxation which may lead to changes in the electronic states. Such distortions are like ones observed in models of small diamond nanoclusters Refs. [13,14] and the surface reconstruction of {111} diamond face [29]. However, in Ref. [29], the electronic structure was calculated using the iterative GW method, which predicted  $\sim 1$  eV energy of the surface states in the surface Brillouin zone (SBZ) due to buckled chains of  $sp^2/sp^3$  atoms formed at reconstruction. The experimental data [30] gave the value of  $\sim 0.5$  eV for the energy of the surface states. Thus, the calculated value of  $\sim 1$  eV for the surface states on reconstructed {111} diamond face [29] is much higher than 0.5 eV obtained experimentally [30]. In contrast to GW, here we used Kohn-Sham eigenvalues and eigenfunctions to calculate the interatomic bond lengths distributions for small-size diamond nanoclusters and the densities of electronic states for the first time.

First the distributions of C—C bond lengths in the clusters of different sizes are calculated as shown in Fig. 3. Each considered cluster is colored according to the bond length values obtained after geometry relaxation. Red color of interatomic bonds in Fig. 3 indicates the lengths less than 1.47 Å, which are attributed to three-coordinated carbon atoms. Black indicates the shortest bonds of 1.235 Å, which connect atoms into carbon chains ( $sp^1$ -bonded atoms) in the outer layer of large clusters (up to 1.7 nm), see Fig. 3d. It is clearly seen that the yellow color bonds, corresponding to  $>1.5$  Å length, relate mostly to the core atoms with four-coordinated carbon atoms (mostly  $sp^3$ -bonds). A part of surface of large clusters is covered by three-coordinated carbon atoms with bond lengths  $<1.5$  Å. This is associated with surface reconstruction and  $sp^2$  hybridized atoms.

Considering the distribution of bond lengths, one can note that the smallest cluster (0.8 nm) exhibits the widest distribution of bond lengths from 1.29 to 1.7 Å, see Fig. 3a). This is due to the small size of the cluster and the dominant role of the surface, which leads to high distortion of the structure. An increase in size to 1 nm (Fig. 3b) results in a bimodal distribution of bond lengths, with those in the core region being bulk-

like ( $>1.5$  Å) and those in surface regions being shorter. Further increases in size up to 1.7 nm led to an increase in the proportion of surface regions with respect to core regions (Fig. 3c–f). Larger the cluster, larger the surface regions and the variety of different C—C bonds. It should be noted that the distribution varies depending on the cluster size, as carbon may form complex surface reconstructions that lead to the formation of different bond types. It is also can be seen that as the cluster sizes increase, the surface  $sp^2$  atoms do not form a continuous layer, but rather islands on the forming faces {111}, which is consistent with the previous simulations [12,13].

Such distortions and changes in the atomic geometry of diamond nanoclusters lead to subsequent changes in electronic properties. To study these changes, we calculated the electronic densities of states (DOS) projected on the core and surface atoms for each cluster. The primary purpose of computed DOS is to demonstrate that the electronic properties of diamond clusters are highly dependent on their size, a phenomenon known as a quantum size effect. For each cluster, the surface and core are defined according to the number of neighbors belonging to each carbon atom. Atoms having three or fewer neighbors are surface atoms, while others with four neighbors are core atoms. Fig. 4 shows the atomic structure of the considered clusters with carbon atoms and bonds, colored according to their core (orange) or surface (blue) regions. In Fig. 4 electronic DOS of core atoms are shown by orange color, while those of surface atoms are blue.

For the smallest cluster of 0.8 nm the gap between the highest occupied level and the lowest unoccupied one is about 0.1 eV, while for 1 nm cluster the gap decreases to 0.015 eV, see Fig. 4. Further increase of the size leads to location of the Fermi level in a subband, so the 1.2 nm cluster exhibits metallic state due to the surface with well-ordered three-coordinated carbon atoms. This emergence of a metallic state is a remarkable deviation from the insulating nature of bulk diamond and underscores the profound influence of surface topology on the electronic structure at the nanoscale. For the 1.5 nm cluster there is a gap of 0.027 eV between the occupied and unoccupied subbands. Thus, the electronic DOS of clusters 1.2 and 1.5 nm (Fig. 4) look very different. The DOS of 1.2 nm cluster is more continuous, while spectra of other clusters contain more distinct bands. Further increase in the size leads to a gap of about 0.040 and 0.032 eV for 1.6 and 1.7 nm clusters respectively. This non-monotonic oscillation of the gap between in-gap energy levels (subbands) with increasing cluster size, rather than smooth progression, indicates that the electronic properties are highly sensitive to specific atomic configurations and quantum confinement effects at low dimensions. Unlike bulk diamond, which has a wide and well-defined band gap ( $\sim 5.5$  eV) such nanoclusters have a set of energy levels and subbands near the Fermi level similarly to the case of the DOS with reduced fundamental gap calculated in Ref. [14] for grain boundaries in ultrananocrystalline diamonds (UNCD). The Fermi level in clusters locates either on the top of the subband ( $D = 0.8, 1.0, 1.5, 1.6, 1.7$  nm), or at the bottom ( $D = 1.2$  nm). Therefore, both p-type and n-type conductivity are possible, depending on the size of diamond nanocluster. This intrinsic ambipolar character is a significant finding, as it suggests that charge transport properties can be selected by controlling the physical size of the nanocluster.

As one can note, the intensities of DOS increase with increasing the cluster size, thus the density of carriers (holes) should increase accordingly. With increasing the size, the DOS develops more defined peaks and valleys. This indicates the formation of more continuous energy bands, which is a signature of the electronic structure transitioning from a molecular-like state with discrete energy levels to a solid-like state. This evolution visualizes the cross-over from a quantum-confined system, where electrons are localized, to a more delocalized band structure. As anticipated, the intensity of subbands related to the core of the clusters decreases as the size of the ND increases. The obtained DOS plots effectively visualize how diamond loses its characteristic insulating properties at the nanoscale and gradually regains them as the cluster size increases, highlighting the transition from quantum dots to bulk

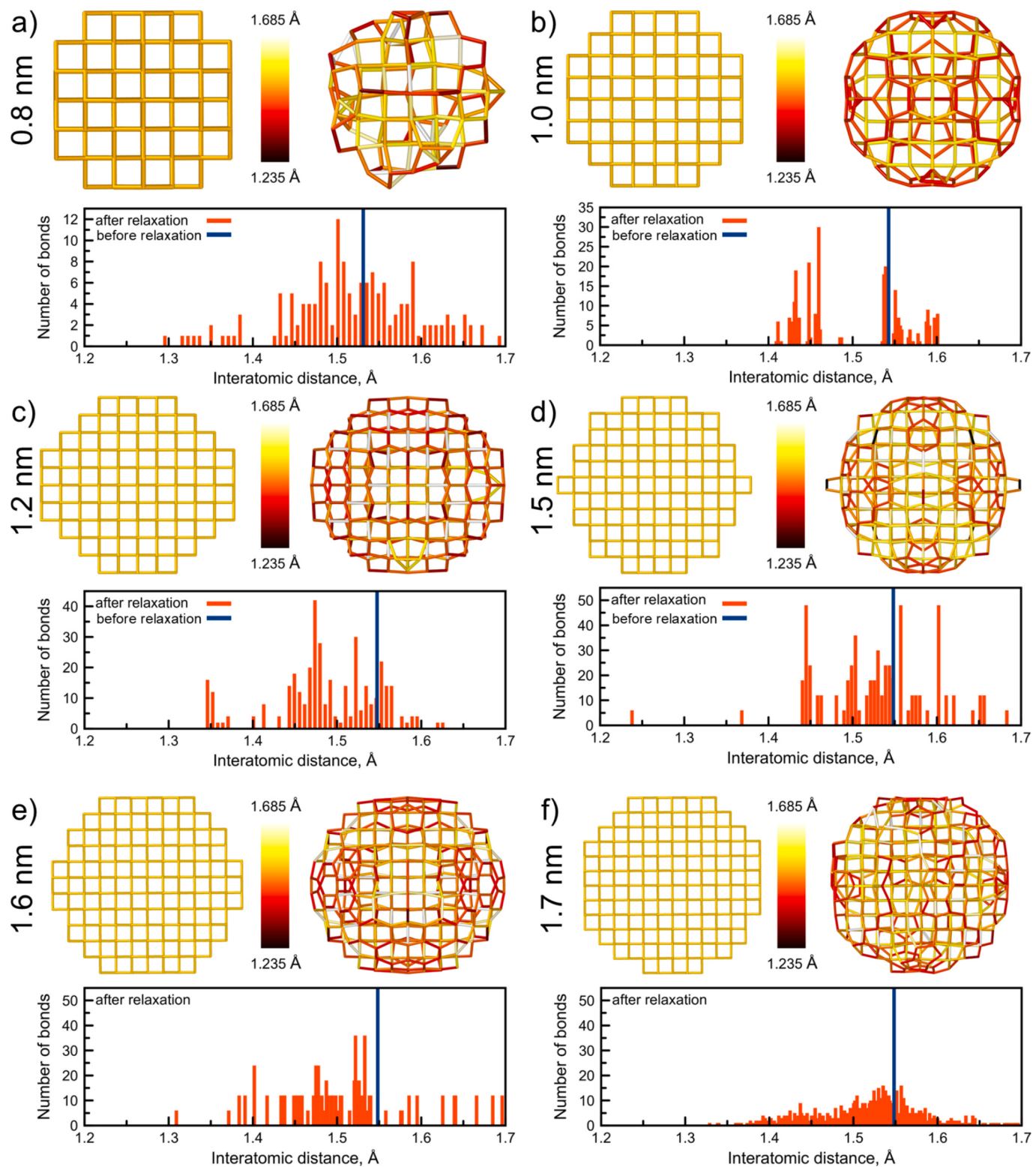


**Fig. 3.** Atomic geometry of unrelaxed  $sp^3$ -bonded diamond cluster, relaxed structure of the cluster, and distributions of the number of interatomic bonds for sizes of a) 0.8, b) 1.0, c) 1.2, d) 1.5 nm, e) 1.6 nm, and f) 1.7 nm. Color of the C—C bonds indicate the length according to the colorbar. Blue vertical line in the distributions of chemical bonds lengths is related to unrelaxed structure.

material. Ultimately, these results paint a complex picture where the electronic properties of nanodiamond are not merely an intermediate state between molecule and solid, but a unique regime where surface chemistry and quantum effects can be harnessed to create new carbon materials with tailored conductivity.

## 6. Discussion

We confirmed that purified detonation nanodiamonds possess semiconductor properties, not semimetallic, which would be in a graphite-like shell covering ND core. The percolation effect in mixtures

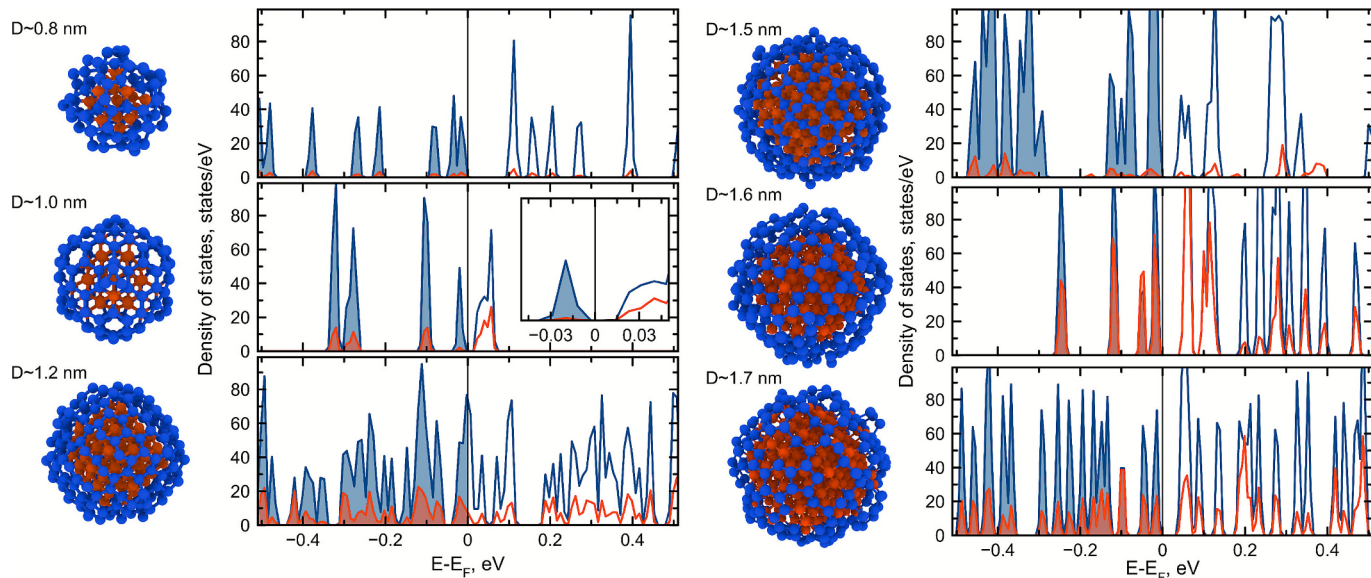


**Fig. 4.** Atomic structure of considered diamond nanoclusters and corresponding electronic density of states projected on the core (orange) and surface (blue) atoms. Fermi energy is set to zero. Occupied energy levels are filled by orange and blue, while unoccupied levels are white.

of conductive and insulator (dielectric) nanopowders usually occurs when the fraction of the conductive component exceeds  $\sim 2$  vol%. The conductive nanoparticles connect in conductive chains [15,16]. When the fraction of the conductive particles is more than  $\sim 15$  vol%, a 3D network on the basis of such chains forms. This kind of nanocomposite can be considered as electrically conductive nanoporous solid with bulk electrical properties similar to the ones of the individual nanoparticles. Thus, the activation energy of charge carriers  $E_a = 0.19 \pm 0.02$  eV of samples with 17, 48, and 59 vol% of DND, Fig. 2, indicates the mean value for individual purified detonation nanodiamonds.

The experimentally obtained value of  $E_a = 0.19 \pm 0.02$  eV in purified DND matches the value of  $0.21 \pm 0.02$  eV found previously on N-doped ultranocrystalline diamond (UNCD) films with  $\sim 10$  nm nanodiamond grain size and  $\sim 1$  nm thick non-diamond intergrain boundaries [31]. In the case of undoped UNCD film much higher value of  $E_a = 0.67 \pm 0.02$  eV was found in the same study. The films of  $3\text{--}12\ \mu\text{m}$  thickness were grown on p-type Si substrates. The low amplitude alternative current technique was used for electrical measurements in [31] as we did. However, the Raman spectra of UNCD films [32] differ significantly from those of purified DND [7,11] due to the non-diamond intergrain boundaries in the films. *Trans*-Polyacetylenes and nanocarbon structures with  $sp^2$  bonds, hybrid  $sp^2/sp^3$  bonds, C—N and other interatomic bonds are present in intergrain boundaries of UNCD [32], these components possess electronic-type transport due to  $\pi$  orbitals of electrons [33].

The multiwave Raman spectra of purified DND in NaCl matrix, which we investigated in this work, were presented earlier in [7]. The spectrum at 257 nm excitation laser in [7] was the same as the one obtained in [11] on purified DND at 244 nm excitation. The sharp diamond line at  $1325\text{--}1326\ \text{cm}^{-1}$  is the strongest in these spectra [7,11], as well as at excitation with 405 nm and 458 nm lasers [7]. The downshifting of the diamond line in DND from the characteristic for larger diamond crystals wavenumber  $1332\ \text{cm}^{-1}$  is attributed to phonon confinement effects in nanocrystals [11]. Contrary to that, diamond line in the Raman spectra of UNCD films is upshifted to  $1336\ \text{cm}^{-1}$ , Ref. [32], as supposed due to compression stresses, and its intensity was much lower than the intensity of the G-band.

Thus, a direct comparison of the electrical properties of purified DND and UNCD films is not valid, since their structures are very different. The matching of  $E_a$  values may be accidental.

We suppose that the observed value of  $E_a = 0.19$  eV relates to the transition from the surface level of  $sp^2$  states occurred due to buckled

$sp^2$ -chains on the reconstructed C(111)  $(2 \times 1)$  surface of ND to the valence band, as was described in [29]. The angle-resolved photoelectron spectroscopy (ARPES) of single crystal boron-doped diamonds [34,30] revealed the energy level attributed to the surface states in the surface Brillouin zone (SBZ) with its maximum at  $0.5 \pm 0.2$  eV below the Fermi level in the SBZ corner (K). The Fermi level locates 1 eV upward the bulk valence band maximum in the Brillouin zone center ( $\Gamma$ ).

The simulations of the ND structure (Fig. 3) and their electronic DOS (Fig. 4) indicate a significant influence of the ND size on the distribution of interatomic bond lengths, the structure of ND and DOS. It should also be noted that for the most “highly symmetric” ND with a diameter of 1 nm, a pronounced bimodal distribution is observed: surface atoms with bond lengths of  $1.42\text{--}1.47\ \text{\AA}$  and bulk-like  $sp^3$  type with bond lengths of  $1.54\text{--}1.60\ \text{\AA}$  (Fig. 3b). Conversely, for the low-symmetric structures with a diameter of 0.8 nm (Fig. 3a), a wide distribution is observed from  $1.29\ \text{\AA}$  to  $1.68\ \text{\AA}$  with a maximum in the region of  $1.5\ \text{\AA}$ , which can be attributed to the  $sp^2\text{-}sp^3$  bond geometry. Bond length distributions for the larger clusters (Fig. 3c–f) are quite different, as well as their visible structure. However, it is possible that if the cluster diameter increases above 2 nm, the bond length distribution depends less on the diameter, and presumably it may also have pronounced bimodal distribution, as in the case of ND with a diameter of 1 nm (Fig. 3b). It can also be assumed that with an increase in the size of the nanocluster from 1.7 nm to more than 2 nm, the calculated energy gap of 0.03 eV will increase to 0.19 eV, which we have found experimentally.

The data obtained on the electronic properties of purified DND may be relevant for applications of these nanoclusters in various types of quantum electronic and optoelectronic devices based on nitrogen-vacancy NV centers. Photoluminescence spectra of both NV<sup>0</sup> and NV<sup>−</sup> centers were revealed after proton bombardment and annealing of purified DND with typical size of 5 nm [35]. The wavenumber of the Raman diamond line of  $1325.4\ \text{cm}^{-1}$  in [35] was the same as in samples which we investigated. Optically detected magnetic resonance (ODMR) spectra indicated isolated NV<sup>−</sup> centers in purified DND [36]. Recently single NV-centers in natural 2–5 nm nanodiamonds of meteoritic origin were identified and the method for their manipulation at the atomic scale using the scanning electron beam presented [37].

## 7. Conclusion

We have investigated the complex electrical conductivity of

detonation diamonds of sizes 2–5 nm in a NaCl dielectric matrix in the temperature range  $T = 300\ldots400$  K and in the frequency range of alternating current  $f = 10^3\ldots10^7$  Hz with a voltage amplitude of 30 mV. The concentration range of ND in the studied samples was 0.16 … 59 vol %. The steps of the frequency dependences of the electrical capacitance  $C(f)$  and the maxima of the reduced conductivity  $G_{\omega}(f)$  at fixed values of  $T$  are revealed, which make it possible to apply the admittance spectroscopy method to determine the activation energy  $E_a$ , the emission rate  $e_n$ , and the capture cross section  $\delta_n$  of the charge carriers in nanodiamonds. The  $E_a$  value was  $0.19 \pm 0.02$  eV for three ND concentrations: 17, 48, and 59 vol%, which is almost the same as  $E_a = 0.21$  eV for an UNCD film with an average diamond grain size of  $\sim 10$  nm grown from a gas mixture with the addition of 5 % nitrogen [31]. The obtained charge carrier capture cross-section  $\delta_n = (2.5 \pm 0.5) \times 10^{-20}$  cm $^2$  and the emission rates  $e_n = 10^3\ldots10^4$  s $^{-1}$  at  $T = 300\ldots400$  K, are similar to highly B-doped diamonds at  $T < 150$  K due to the hopping conduction via the impurity subband [18]. The value of the specific conductivity of detonation diamonds at  $T = 300$  K is  $\sim 10^{-6}$  Ω $^{-1}$  cm $^{-1}$ , which is about 4 orders of magnitude less than in UNCD film with an average diamond grain size of  $\sim 5$  nm and a grain boundary thickness of  $\sim 0.5$  nm grown from a gas mixture containing 1 % N<sub>2</sub> [33]. The estimated concentration of charge carriers at  $T = 300$  K is  $\sim (10^{12}\ldots10^{13})$  cm $^{-3}$ . Density functional theory calculations were performed to analyze the electronic properties of diamond nanocluster depending on the size. Nanoclusters with a diameter of 0.8, 1.0, 1.2, 1.5, 1.6 and 1.7 nm were considered, and structural properties and electronic density of states were computed and analyzed. The computed distributions of the number of interatomic bonds by their length indicate the structural features of nanoclusters depending on their size. The obtained electronic DOS contains allowed

energy levels and subbands in the vicinity of the Fermi level due to the presence of carbon chains with  $sp^2$  bonds similar to grain boundaries considered in [14]. Such chains in ND are located on their surface and, accordingly, can form levels of the surface states in the band gap, the models of which were studied in [29,30]. The obtained data on the structure and electronic properties of small-size nanodiamonds can be used in the development of quantum devices based on single NV centers in diamonds, as well as arrays of such ND with single NV centers.

#### CRediT authorship contribution statement

**S.G. Buga:** Writing – review & editing, Writing – original draft, Validation, Methodology, Investigation, Formal analysis, Data curation, Conceptualization. **M.Yu. Popov:** Validation, Investigation, Formal analysis. **D.A. Ovsyannikov:** Resources. **V.S. Baidyshev:** Investigation, Data curation. **A.G. Kvashnin:** Writing – review & editing, Writing – original draft, Visualization, Validation, Investigation, Formal analysis, Data curation.

#### Declaration of competing interest

The authors declare that they have no known competing financial interests or personal relationships that could have appeared to influence the work reported in this paper.

#### Acknowledgments

Equipment provided by the TISNUM collective use center ([www.tisnum.ru/suec/suec.html](http://www.tisnum.ru/suec/suec.html)) was used in the study.

## Appendix A

### Equivalent electrical circuit of the samples

Studies of the Cole-Cole diagrams of the electrical impedance of the samples allowed us to determine the type of equivalent electrical circuit of the samples shown in Fig. A1a). This equivalent scheme is evidenced by the examples of Cole-Cole diagrams shown in Fig. A1b–d).

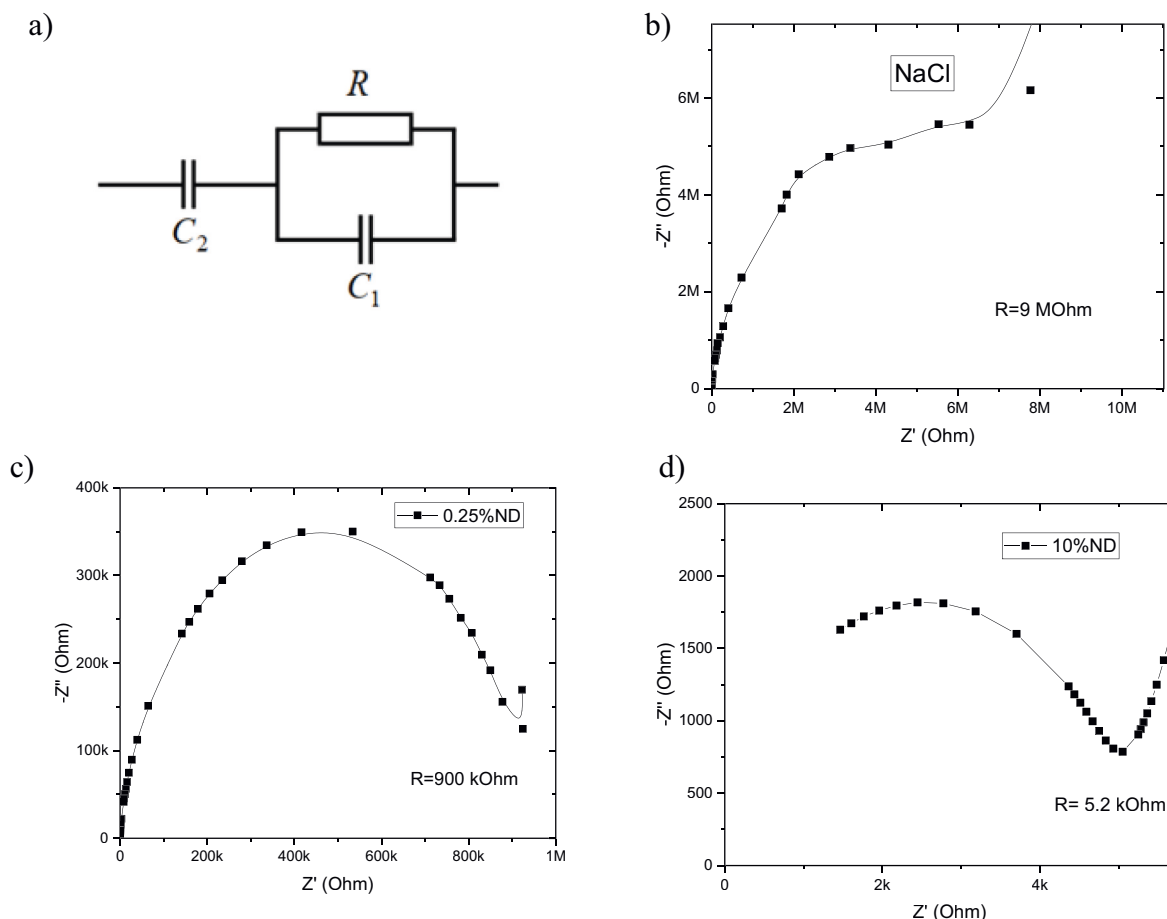


**Fig. A1.** Equivalent electrical circuit of the measured samples (a). Examples of Cole-Cole diagrams of the electrical impedance of NaCl sample (b); NaCl+0.16 vol% ND: (c), and NaCl+6.3 vol% ND: (d) at  $T = 295$  K.

To plot the Cole-Cole diagrams, Fig. A1b–d), measurements of the frequency dependences of electrical resistance  $R(f)$  and capacitance  $C(f)$  were performed, on the basis of which the real and imaginary parts of the electrical impedance  $Z'(\omega) = R(\omega)$  and  $Z''(\omega) = -1/\omega C(\omega)$  were calculated, where  $\omega = 2\pi f$  is the angular frequency. The values of  $Z'(\omega)$  and  $Z''(\omega)$  obtained in this way did not differ significantly from those calculated using formulas for a parallel connection equivalent electrical circuit:  $Z' = \frac{R_p}{1 + (\omega C_p R_p)^2}$ ;  $Z'' = \frac{-\omega C_p R_p^2}{1 + (\omega C_p R_p)^2}$

This means that  $C_2 \gg C_1$ , since at series connection of capacitors their total capacitance is determined by the one that is much smaller, and in this case, the capacitance of  $C_2$  can be neglected. Subsequently, in accordance with the determined equivalent electrical circuit and the assumption  $C_2 \gg C_1$ , the electrical conductance  $G$  (electrical admittance  $Y'$ ) and capacitance  $C$  (component of the imaginary part of admittance  $Y'' = -\omega C$ ) of the samples were measured. This made it possible to analyze the experimental data obtained using the method of admittance spectroscopy of semiconductors, as well as to estimate the density of charge carriers at room temperature.

The ratio  $C_2 \gg C_1$  is also consistent with the fact that the capacity of diamond nanoparticles is proportional to their radius  $r$  ( $C = 4\pi\epsilon\epsilon_0 r$ ), where  $\epsilon$  and  $\epsilon_0$  are the dielectric constant of diamond and vacuum, respectively), and NaCl powder, due to its plasticity, does not form nanoparticles during ball milling and further compaction, but represents a thin layer between ND particles and metal contacts, the capacitance of which is inversely proportional to the thickness of  $t_i$  ( $C = \epsilon\epsilon_0 S/t_i$ ), where  $S$  is the contact area), and  $t_i$  has the same order of magnitude as  $r$  at not very small ratios of volume fractions of ND and NaCl in the sample.

## Data availability

Data will be made available on reasonable request.

## References

- [1] T. Tegafaw, S. Liu, M.Y. Ahmad, A. Khamis, A.A. Saidi, D. Zhao, Y. Liu, H. Yue, S.-W. Nam, Y. Chang, G.H. Lee, Production, surface modification, physicochemical properties, biocompatibility, and bioimaging applications of nanodiamonds, RSC Adv. 13 (2023) 32381–32397, <https://doi.org/10.1039/d3ra06837a>.
- [2] O.A. Shenderova, A.I. Shames, N.A. Nunn, M.D. Torelli, I. Vlasov, A. Zaitsev, Review article: synthesis, properties, and applications of fluorescent diamond particles, J. Vac. Sci. Technol. B 37 (2019) 030802, <https://doi.org/10.1116/1.5089898>.
- [3] P.I. Belobrov, L.A. Bursill, K.I. Maslakov, A.P. Dementjev, Electron spectroscopy of nanodiamond surface states, Appl. Surf. Sci. 215 (2003) 169–177, [https://doi.org/10.1016/S0169-4332\(03\)00287-3](https://doi.org/10.1016/S0169-4332(03)00287-3).
- [4] X. Fang, J. Mao, E.M. Levin, K. Schmidt-Rohr, Nonaromatic core-shell structure of nanodiamond from solid-state NMR spectroscopy, J. Am. Chem. Soc. 131 (2009) 1426–1435, <https://doi.org/10.1021/ja8054063>.
- [5] M. Popov, V. Churkin, A. Kirichenko, V. Denisov, D. Ovsyannikov, B. Kulnitskiy, I. Perezhogin, V. Aksenenkov, V. Blank, Raman spectra and bulk modulus of nanodiamond in a size interval of 2–5 nm, Nanoscale Res. Lett. 12 (2017) 561, <https://doi.org/10.1186/s11671-017-2333-0>.
- [6] M. Popov, V. Churkin, D., Ovsyannikov, A. Khabibrakhmanov, A. Kirichenko, E. Skryleva, Yu. Parkhomenko, M. Kuznetsov, S. Nosukhin, P. Sorokin, S. Terentiev, V. Blank. Ultrasmall diamond nanoparticles with unusual incompressibility. Diamond Relat. Mater. 96 (2019) 52–57. doi:<https://doi.org/10.1016/j.diamond.2019.04.033>.

- [7] M. Popov, F. Khorobrykh, S. Klimin, V. Churkin, D. Ovsyannikov, A. Kvashnin, Surface Tamm states of 2-5 nm nanodiamond via Raman spectroscopy, *Nanomaterials* 13 (2023) 696, <https://doi.org/10.3390/nano13040696>.
- [8] V.L. Kuznetsov, M.N. Aleksandrov, I.V. Zagoruiko, A.L. Chuvilin, E.M. Moroz, V. N. Kolomiichuk, V.A. Likholobov, P.M. Brylyakov, G.V. Sakovitch, Study of ultradispersed diamond powders obtained using explosive energy, *Carbon* 29 (1991) 665–668.
- [9] V. Dolmatov, M. Veretennikova, V. Marchukov, V. Sushchev, Currently available methods of industrial nanodiamond synthesis, *Phys. Solid State* 46 (2004) 611–615.
- [10] A. Krueger, The structure and reactivity of nanoscale diamond, *J. Mater. Chem.* 18 (2008) 1485–1492.
- [11] I.I. Vlasov and O.A. Shenderova Raman and Photoluminescence Spectroscopy of Detonation Nanodiamonds, Chapter 5 in “Detonation Nanodiamonds: Science and Applications” Eds. A.Ya. Vul’ and O.A. Shenderova. Copyright 2014 Pan Stanford Publishing Pte. Ltd. ISBN 978-981-4411-27-1 (Hardcover), 978-981-4411-28-8 (eBook).
- [12] A.S. Barnard, M. Sternberg, Crystallinity and surface electrostatics of diamond nanocrystals, *J. Mater. Chem.* 17 (2007) 4811–4819, <https://doi.org/10.1039/b710189a>.
- [13] S.L.Y. Chang, C. Dwyer, E. Osawa, A.S. Barnard, Size dependent surface reconstruction in detonation nanodiamond, *Nanoscale Horiz.* 3 (2018) 213–217, <https://doi.org/10.1039/C7NH00125H>.
- [14] F. Cleri, P. Kebelinski, L. Colombo, D. Wolf, S.R. Phillpot, On the electrical activity of sp<sub>2</sub>-bonded grain boundaries in nanocrystalline diamond, *Europhys. Lett.* 46 (5) (1999) 671–677. <http://iopscience.iop.org/0295-5075/46/5/671>.
- [15] N.A. Poklonskiy, N.I. Gorbachuk, Fundamentals of impedance spectroscopy of composites 130, Belarus St. Univ., Minsk, 2005 (in Russian), ISBN 985-485-457-4, [https://www.studmed.ru/poklonskiy-na-gorbachuk-ni-osnovy-impedansnoy-spektroskopii-kompozitov-kurs-lekciy\\_4313734ab10.html](https://www.studmed.ru/poklonskiy-na-gorbachuk-ni-osnovy-impedansnoy-spektroskopii-kompozitov-kurs-lekciy_4313734ab10.html).
- [16] J.V. Li, G. Ferrari (Eds.), Capacitance Spectroscopy of Semiconductors, Pan Stanford Publishing Pte. Ltd, 2018, ISBN 978-1-315-15013-0.
- [17] Y. Koide, S. Koizumi, H. Kanda, M. Suzuki, H. Yoshida, N. Sakuma, T. Ono, T. Sakai, Admittance spectroscopy for phosphorus-doped n-type diamond epilayer, *Appl. Phys. Lett.* 86 (2005) 232105, <https://doi.org/10.1063/1.1944896>.
- [18] V.I. Zubkov, O.V. Kucherova, S.A. Bogdanov, A.V. Zubkova, J.E. Butler, V.A. Ilyin, A.V. Afanas’ev, A.L. Vikharev, Temperature admittance spectroscopy of boron doped chemical vapor deposition diamond, *J. of Appl. Phys.* 118 (2015) 145703, <https://doi.org/10.1063/1.4932664>.
- [19] V.I. Zubkov, A.V. Solominika, J.E. Post, E. Gaillou, J.E. Butler, Characterization of electronic properties of natural type IIb diamonds, *Diamond & Related Materials* 72 (2017) 87–93, <https://doi.org/10.1016/j.diamond.2017.01.011>.
- [20] G. Vincent, D. Bois, P.J. Pinard, Conductance and capacitance studies in GaP Schottky barriers, *Appl. Phys.* 46 (1975) 5173–5178, <https://doi.org/10.1063/1.322194>.
- [21] P. Hohenberg, W. Kohn, Inhomogeneous electron gas, *Phys. Rev. B* 136 (3) (1964) B864–B871, <https://doi.org/10.1103/PhysRev.136.B864>.
- [22] W. Kohn, L.J. Sham, Self-consistent equations including exchange and correlation effects //, *Phys. Rev.* 140 (4) (1965) A1133–A1138, <https://doi.org/10.1103/PhysRev.140.A1133>.
- [23] G. Kresse, J. Furthmüller, Efficient iterative schemes for ab initio total-energy calculations using a plane-wave basis set, *Phys. Rev. B* 54 (16) (1996) 11169–11186.
- [24] G. Kresse, J. Hafner, Ab initio molecular dynamics for liquid metals, *Phys. Rev. B* 47 (1993) 558–561, <https://doi.org/10.1103/PhysRevB.54.11169>.
- [25] G. Kresse, J. Hafner, Ab initio molecular-dynamics simulation of the liquid-metal-amorphous-semiconductor transition in germanium, *Phys. Rev. B* 49 (20) (1994) 14251–14269, <https://doi.org/10.1103/PhysRevB.49.14251>.
- [26] J.P. Perdew, K. Burke, M. Ernzerhof, Generalized gradient approximation made simple, *Phys. Rev. Lett.* 77 (18) (1996) 3865–3868, <https://doi.org/10.1103/PhysRevLett.77.3865>.
- [27] P.E. Blöchl, Projector augmented-wave method, *Phys. Rev. B* 50 (24) (1994) 17953–17979, <https://doi.org/10.1103/PhysRevB.50.17953>.
- [28] G. Kresse, D. Joubert, From ultrasoft pseudopotentials to the projector augmented-wave method, *Phys. Rev. B* 59 (3) (1999) 1758–1775, <https://doi.org/10.1103/PhysRevB.59.1758>.
- [29] O. Pulci, M. Marsili, P. Gori, M. Palummo, A. Criventi, F. Bechstedt, R. del Sole, Geometry and electronic band structure of surfaces: the case of Ge(111):Sn and C (111), *Appl. Phys. A Mater. Sci. Process* 85 (2006) 361–369. <https://link.springer.com/content/pdf/10.1007/s00339-006-3694-x.pdf>.
- [30] R. Graupner, M. Hollering, A. Ziegler, J. Ristein, L. Ley, A. Stampfl, Dispersions of surface states on diamond (100) and (111), *Phys. Rev. B* 55 (1997) 10841–10847, <https://doi.org/10.1103/PhysRevB.55.10841>.
- [31] M.C. Feliciangeli, M.C. Rossi, G. Conte, V. Ralchenko, Nitrogen-doped ultrananocrystalline carbon: Response to small amplitude AC signals, *Physica E* 40 (2008) 2583–2588, <https://doi.org/10.1016/j.physe.2007.10.059>.
- [32] I.I. Vlasov, V.G. Ralchenko, E. Goovaerts, A.V. Saveliev, M.V. Kanzyuba, Bulk and surface-enhanced Raman spectroscopy of nitrogen-doped ultrananocrystalline diamond films, *Physica Status Solidi (A)* 203 (12) (2006) 3028–3035, <https://doi.org/10.1002/pssa.200671119>.
- [33] S. Bhattacharyya, O. Auciello, J. Birrell, J. A. Carlisle, L. A. Curtiss, A. N. Goyette, D. M. Gruen, A. R. Krauss, J. Schlüter, A. Suman, and P. Zapal. Synthesis and characterization of highly-conducting nitrogen-doped ultrananocrystalline diamond films. *Appl. Phys. Lett.* 79 (2001) 1441 doi:<https://doi.org/10.1063/1.1400761>.
- [34] F.J. Himpsel, D.E. Eastman, P. Heimann, J.F. van der Veen, Surface states on reconstructed diamond (111), *Phys. Rev. B* 24 (1981) 7270, <https://doi.org/10.1103/PhysRevB.24.7270>.
- [35] B.R. Smith, D.W. Inglis, B. Sandnes, J.R. Rabeau, A.V. Zvyagin, D. Gruber, C. J. Noble, R. Vogel, E. Osawa, T. Plakhotnik, Five-nanometer diamond with luminescent nitrogen-vacancy defect centers, *Small* 5 (2009) 1649–1653, <https://doi.org/10.1002/smll.200801802>.
- [36] C. Bradac, T. Gaebel, N. Naidoo, M.J. Sellars, J. Twamley, L.J. Brown, A.S. Barnard, T. Plakhotnik, A.V. Zvyagin, J.R. Rabeau, Observation and control of blinking nitrogen-vacancy centres in discrete nanodiamonds, *Nat. Nanotechnol.* 5 (2010) 345–349, <https://doi.org/10.1038/nnano.2010.56>.
- [37] B.M. Hudak, R.M. Stroud, Atomically precise detection and manipulation of nitrogen-vacancy centers in nanodiamonds, *ACS Nano* 17 (2023) 7241–7249, <https://doi.org/10.1021/acsnano.2c10122>.